Research Article

Segmented predictor-corrector reentry guidance based on an analytical profile

Hui XU[1], Guangbin CAI[1✉], Chaoxu MU[2], Xin LI[1], Hao WEI[1]

[1]*Department of Missile Engineering, Rocket Force University of Engineering, Xi'an 710025, China*
[2]*School of Electrical and Information Engineering, Tianjin University, Tianjin 300072, China*

Abstract: A segmented predictor-corrector method is proposed for hypersonic glide vehicles to address the issue of the slow computational speed of obtaining guidance commands using the traditional predictor-corrector guidance method. Firstly, an altitude-energy profile is designed, and the bank angle is derived analytically as the initial iteration value for the predictor-corrector method. The predictor-corrector guidance method has been improved by deriving an analytical form for predicting the range-to-go error, which greatly accelerates the iterative speed. Then, a segmented guidance algorithm is proposed. The above analytically predictor-corrector guidance method is adopted when the energy exceeds an energy threshold. When the energy is less than the threshold, the equidistant test method is used to calculate the bank angle command, which ensures guidance accuracy as well as computational efficiency. Additionally, an adaptive guidance cycle strategy is applied to reduce the computational time of the reentry guidance trajectory. Finally, the accuracy and robustness of the proposed method are verified through a series of simulations and Monte Carlo experiments. Compared with the traditional integral method, the proposed method requires 75% less computation time on average and achieves a lower landing error.

Keywords: Hypersonic glide vehicle; Segmented reentry guidance method; Analytical profile; Adaptive guidance cycle; Reentry trajectory

1 Introduction

Hypersonic glide vehicles (HGVs) have attracted great attention due to their fast global strike capability and super maneuverability (Zhang et al., 2015; Tauqer et al., 2015; Chen et al., 2020; An et al., 2022). A series of reliable guidance systems is needed to ensure that an HGV reaches the target accurately. However, the characteristics of nonlinearity, strong coupling, and fast dynamics throughout the HGV reentry flight bring huge challenges to online guidance (Shen and Lu, 2003; Gao et al., 2019). As well as satisfying the usual path constraints such as the heating rate, aerodynamic load, and dynamic pressure during flight, the quasi-equilibrium glide condition (QEGC) must be satisfied for some special

reentry tasks (Zhang et al., 2019; Gao et al., 2020; Lu, 2014). An effective guidance method is required to complete the guidance task well with multiple and strict constraints.

Conventional reentry guidance methods are divided into standard trajectory and predictor-corrector guidance methods (Liang and Zhu, 2021; Zeng et al., 2018; Wang, 2017). The standard trajectory method needs to design the reference trajectory offline. The aircraft can hit the target by tracking the standard trajectory online with a carefully designed tracker, but the method is not flexible when used for reentry cases with high uncertainty and a changed target. The predictive correction guidance algorithm is a guidance algorithm widely studied in recent years, and has strong versatility and robustness. It adapts to different reentry missions and does not need to design the reference trajectory in advance. A predictor-corrector guidance algorithm usually guides flight vehicles accurately to the target point by continuously predicting the difference between the terminal

✉ Guangbin CAI, cgb0712@163.com

flight state and the expected state (Lu, 2008; Wang, 2017). A numerical predictor-corrector method for the path constraints was discussed and proposed by Joshi et al. (2007). Xue and Lu (2010) proposed a good strategy in which path constraints are transformed into the magnitude limit of the bank angle when conducting the predictor-corrector method. However, there are some problems with the above methods. In the prediction process, when the target point is far away, the numerical integration method will involve a huge amount of calculation, which seriously affects the real-time performance and computational efficiency of the algorithm (Xia et al., 2015; Yong et al., 2014; Li and Hu, 2018; Zhou et al., 2020). To solve these problems, the selection of path points for predictor-corrector guidance was proposed. The predictor link stops at the selected path points, thereby shortening the calculation time, but the accessibility of these path points cannot be guaranteed. Liang et al. (2017) proposed a virtual terminal-based adaptive predictor-corrector entry guidance method. Once a vehicle reaches the virtual target point, the predictor-corrector guidance switches automatically to the reference trajectory tracking method. The main component of these methods is numerical integration predictor-corrector guidance, and computational efficiency is still a factor that must be considered in practical application. In the process of studying no-fly zone avoidance guidance, a segmented predictor-corrector guidance method was proposed to improve guidance accuracy and computational efficiency. Different terminal state errors are used as objective functions in different guidance stages (Zhang et al., 2021). In recent years, an analytical predictor-corrector guidance method has also been studied which can obtain the predicted value with a small calculation and good real-time performance (Zeng et al., 2013; Wang et al., 2019; Yu et al., 2018; Pan et al., 2019). However, the accuracy and adaptability of this method need to be improved due to different simplifications.

To address this issue, a segmented analytical predictor-corrector reentry guidance method is proposed in this paper. The whole prediction guidance process is divided into two phases based on a preset energy threshold. In the first phase, the range-to-go error, obtained by an analytical expression related to the bank angle and energy, is selected as the objec-

tive function. This can greatly reduce the computational burden of using numerical integration. In the second phase, since the target point is relatively close, the equidistant division test method is used to obtain the bank angle to further improve guidance accuracy, and the landing point deviation is calculated by the numerical integration method. Additionally, a novel altitude-energy profile is proposed. The bank angle is analytically derived, and is used as the initial value of the bank angle iteration in the predictor-corrector link. The adaptive guidance cycle strategy is used to optimize the guidance command generation process. Experiments were conducted to verify the effectiveness and robustness of the proposed guidance method.

The novelties of the algorithm proposed in this paper are as follows:

(1) A new altitude-energy profile is designed, and the magnitude of the bank angle is derived analytically, which provides a good initial value for iterative computations in the predictor-corrector guidance method.

(2) An analytical method for predicting the range-to-go error is derived, which greatly reduces the computational time required for the predictor-corrector link.

(3) A method of segmented guidance combined with an adaptive guidance cycle is proposed to further accelerate the calculation of the reentry guidance trajectory and improve guidance accuracy.

(4) Simulation results show that the algorithm is fast and accurate, and has the potential for online application.

The rest of this paper is organized as follows: Section 2 introduces the reentry guidance problem formulation. The novel guidance law is described in Section 3. Several series of simulations conducted to verify the advantages of the proposed method are described in Section 4. Conclusions are drawn in Section 5.

2 Reentry trajectory optimization problem formulation

2.1 Dynamic model of HGV

The three-dimensional point-mass dynamics of an HGV are given by (Gao et al., 2019):

$$\begin{cases} \dot{r} = V \sin \gamma \\ \dot{\theta} = \dfrac{V \cos \gamma \sin \psi}{r \cos \phi} \\ \dot{\phi} = \dfrac{V \cos \gamma \cos \psi}{r} \\ \dot{V} = -\dfrac{D}{m} - g \sin \gamma \\ \dot{\gamma} = \dfrac{L \cos \sigma}{mV} - \left(\dfrac{g}{V} - \dfrac{V}{r} \right) \cos \gamma \\ \dot{\psi} = \dfrac{L \sin \sigma}{mV \cos \gamma} + \dfrac{V}{r} \cos \gamma \sin \psi \tan \phi \end{cases} \tag{1}$$

where r is the radial distance between the Earth center and the vehicle; θ represents the longitude; ϕ is the latitude; V is the velocity magnitude, and γ, ψ represent the flight path angle and the heading angle, respectively; m is the mass of the HGV; g is the acceleration of gravity; L and D denote the aerodynamic lift force and the drag force, respectively. The control variable σ represents the bank angle and α represents the AOA. L and D take the form of:

$$\begin{cases} D = c_D q S \\ L = c_L q S \end{cases} \tag{2}$$

where c_D and c_L represent the aerodynamic drag coefficient and lift coefficient, respectively, which are affected by the AOA α and the March number *Ma* (Xu et al., 2021). S is the characteristic area of the hypersonic flight, and q is the dynamic pressure, which are calculated by:

$$\begin{cases} q = \dfrac{\rho V^2}{2} \\ \rho = \rho_0 e^{-\beta h} \end{cases} \tag{3}$$

where ρ is the atmospheric density, $\rho_0 = 1.225 \mathrm{kg/m^3}$ and $\beta = 1.406e - 4 \ \mathrm{m^{-1}}$, h is the altitude and $h = r - R$, and the constant R is the Earth radius.

At the reentry phase, an energy function is introduced to simplify the dynamics and is used as the stopping criterion for the reentry phase. The energy function takes the form of:

$$E = \frac{\mu}{r} - \frac{V^2}{2} \tag{4}$$

where μ is the gravitational parameter. The differential of the energy E can be expressed as:

$$\begin{aligned} \frac{\mathrm{d}E}{\mathrm{d}t} &= -\frac{\mu}{r^2} \cdot \frac{\mathrm{d}r}{\mathrm{d}t} - V \frac{\mathrm{d}V}{\mathrm{d}t} \\ &= -gV \sin \gamma - V \left(-\frac{D}{m} - g \sin \gamma \right) \\ &= \frac{DV}{m} \end{aligned} \tag{5}$$

Therefore, combined with Eq. (5), Eq. (1) can be transferred as follows:

$$\begin{cases} \dfrac{\mathrm{d}r}{\mathrm{d}E} = \dfrac{m \sin \gamma}{D} \\ \dfrac{\mathrm{d}\theta}{\mathrm{d}E} = \dfrac{m \cos \gamma \sin \psi}{Dr \cos \phi} \\ \dfrac{\mathrm{d}\phi}{\mathrm{d}E} = \dfrac{m \cos \gamma \cos \psi}{Dr} \\ \dfrac{\mathrm{d}\gamma}{\mathrm{d}E} = \dfrac{L \cos \sigma - \left(mg - \dfrac{mV^2}{r} \right) \cos \gamma}{DV^2} \\ \dfrac{\mathrm{d}\psi}{\mathrm{d}E} = \dfrac{L \sin \sigma + \dfrac{mV^2}{r} \cos^2 \gamma \sin \psi \tan \phi}{DV^2 \cos \gamma} \end{cases} \tag{6}$$

2.2 Trajectory constraints

During the reentry flight, some typical inequality path constraints need to be satisfied, which are given by:

$$\begin{cases} q = 0.5 \rho V^2 \le q_\mathrm{m} \\ \bar{n} = \dfrac{\sqrt{L^2 + D^2}}{mg_0} \le n_\mathrm{m} \\ \dot{Q} = K_Q \rho^{0.5} V^{3.15} \le \dot{Q}_\mathrm{m} \end{cases} \tag{7}$$

where q_m, n_m, and $\dot{Q}_\mathrm{m}$ are the maximum allowable values of the dynamic pressure, the aerodynamic load, and the heating rate, respectively. $K_Q = 7.9686 \times 10^{-5}$ is a constant with respect to the structural property of the HGV.

Recently, the QEGC has been studied as a soft constraint to obtain the flatness of the trajectory, which is given by:

$$(mg - \frac{mV^2}{r}) \cos \gamma - L \cos \sigma = 0 \tag{8}$$

For an HGV, the desired terminal conditions are different because of the different flight missions. With the energy as the independent variable, the typical terminal constraints are given by:

$$\begin{cases} r(E_{\mathrm{f}}) = r_{\mathrm{f}} \\ V(E_{\mathrm{f}}) = V_{\mathrm{f}} \\ s(E_{\mathrm{f}}) = s_{\mathrm{f}} \end{cases} \tag{9}$$

where r_{f}, V_{f}, s_{f} are the expected altitude, velocity, and the range-to-go, respectively. E_{f} is the terminal energy with respect to the terminal altitude and velocity. The range-to-go is calculated by:

$$s = R * \arccos(\sin\phi_{\mathrm{f}} \sin\phi + \cos\phi_{\mathrm{f}} \cos\phi \cos(\theta_{\mathrm{f}} - \theta)) \tag{10}$$

where θ_{f}, ϕ_{f} are the expected terminal longitude and latitude. In the simulation experiment, in which the reentry task had target point allowable deviation, terminal range-to-go constraints were expressed as:

$$\Delta s(E_{\mathrm{f}}) \leq \Delta s_{\mathrm{f}} \tag{11}$$

where $\Delta s(E_{\mathrm{f}})$ is the actual range-to-go error at E_{f}, Δs_{f} is the allowable error.

3 Segmented predictor-corrector guidance based on the analytical profile

The predictor-corrector guidance method is divided mainly into the prediction stage and the command correction stage, which can eliminate the deviation between the predicted and desired landing points and ensure that the vehicle accurately reaches the target point. In the prediction stage, numerical integration is generally used to predict the final landing point and then calculate the deviation from the target point. However, at the start the reentry flight is far away from the target point, and the numerical integration method may involve a huge amount of computation, which seriously affects the real-time performance of the algorithm.

To solve this problem, we propose a segmented strategy for the predictor-corrector algorithm. When the energy is greater than the set threshold, an analytical method is derived to calculate the deviation of the landing point based on the energy variable, greatly reducing the computational burden of the traditional method. When the energy is less than the threshold, the vehicle is close to the target point, and it is feasible to use the numerical integration method to obtain the fall point deviation. The isometric-trial method is used to obtain the bank angle command. In addition, a novel altitude-energy profile is proposed to derive the bank angle magnitude analytically. This angle is used as the initial value of the bank angle

iteration in the correction stage.

3.1 Longitudinal guidance

In this study, as in the shuttle entry trajectory planning, we designed the optimal AOA profile as a piecewise linear function of velocity, which takes the following form:

$$\alpha = \begin{cases} \alpha_{\max}, & V_1 < V \leq V_0 \\ \dfrac{(\alpha_{\mathrm{ratio}} - \alpha_{\max})}{V_2 - V_1} \cdot (V - V_1) + \alpha_{\max}, & V_2 < V \leq V_1 \\ \alpha_{\mathrm{ratio}}, & V_{\mathrm{f}} \leq V \leq V_2 \end{cases} \tag{12}$$

where $\alpha_{\max}$ is the maximal AOA, α_{ratio} is the maximal lift-to-drag AOA, V_0 and V_{f} represent the beginning and the terminal velocity, respectively. V_1 and V_2 are two parameters designed to optimize the AOA curve.

3.1.1 Analytical derivation of the predictive range-to-go error

When the energy is very large, it indicates that the vehicle is in the early stage of reentry flight. If the numerical integration method is used to calculate the range-to-go, it will involve a huge amount of calculation. To avoid this problem, an analytical method for calculating the range-to-go is applied.

The derivative of the range-to-go can generally be expressed as:

$$\frac{\mathrm{d}s}{\mathrm{d}t} = -V cos\gamma \tag{13}$$

With energy as the independent variable, Eq. (13) can be transformed into:

$$\frac{\mathrm{d}s}{\mathrm{d}E} = -V cos\gamma * \frac{m}{DV} = -\frac{m cos\gamma}{D} \tag{14}$$

There is the following relationship between D and L:

$$D = \frac{L}{c_{\mathrm{L}}} * c_{\mathrm{D}} \tag{15}$$

From Eq. (8), L has the following form:

$$L = m(g - \frac{V^2}{r}) * \frac{cos\gamma}{cos\sigma} \tag{16}$$

Therefore, combining Eqs. (4), (14), (15), and (16), the derivative of s with respect to E:

$$\frac{\mathrm{d}s}{\mathrm{d}E} = \frac{-m\cos\gamma}{m(g-\frac{V^2}{r})*\frac{\cos\gamma}{\cos\sigma}*\frac{c_D}{c_L}}$$

$$= -\frac{\eta r*\cos\sigma}{gr-V^2} = -\frac{\eta r*\cos\sigma}{\frac{\mu}{r^2}r-(\frac{2\mu}{r}-2E)} = \frac{\eta r*\cos\sigma}{\frac{\mu}{r}-2E} \qquad (17)$$

where $\eta = \frac{c_L}{c_D}$ represents the lift-drag ratio. Assuming that the changes of η and r can be ignored, the deviation of the predicted drop point at the current moment is:

$$s_p(E_f) = s(E_c) + \int_{E_c}^{E_f} -\frac{\eta r*\cos\sigma}{2E-\frac{\mu}{r}}dE$$

$$= s(E_c) - \frac{\eta r\cos\sigma}{2}*\ln(\frac{2E_f-\frac{\mu}{r}}{2E_c-\frac{\mu}{r}}) \qquad (18)$$

where E_c is current energy; $s(E_c)$ is the range-to-go at the current moment. $s_p(E_f)$ is the predicted terminal range-to-go at the current moment calculated analytically by Eq. (18), which greatly reduces the amount of computation burden to obtain the predicted landing point by traditional numerical integration.

3.1.2 Instruction corrector based on segmented objective function

The corrector of command is generally solved by the secant method or Newton iteration method. However, when the flight vehicle is close to the terminal time, the method of predicting the range-to-go error with the analytical method leads to large deviations and frequent switching of the bank angle. As the distance from the target point decreases, the prediction accuracy of the landing point by the numerical integration increases, and the calculation amount is acceptable. Therefore, the following segmented objective function was used in this study:

$$f = \begin{cases} s_{pf}, E > E_s \\ s_{ft}, E \le E_s \end{cases} \qquad (19)$$

where s_{pf} is the terminal predicted range-to-go calculated analytically by Eq. (18); s_{ft} is the landing point error between the prediction landing point and the target point calculated by the equidistant test method; E_s represents the transfer value switch of the objective function designed for the novel guidance

method.

To improve the efficiency of iteratively solving the magnitude of the bank angle, a new altitude-energy profile is proposed, and the altitude, velocity, flight path angle and bank angle can be derived through analysis. The obtained bank angle is used as the initial value of the correction link to further reduce the amount of calculation. The altitude-energy profile is designed as follows:

$$h = F(e) = \sum_{i=1}^{n} a_i e^{i-1} \qquad (20)$$

where a_i represents the coefficients of the five-order polynomial and e is the nondimensional energy expressed as:

$$e = \frac{E-E_0}{E_f-E_0} \qquad (21)$$

Then, considering Eq. (6), the first- and second-order derivatives of Eq. (20) are as follows:

$$\frac{\mathrm{d}h}{\mathrm{d}e} = \sum_{i=2}^{n}(i-1)a_i e^{i-2} = \frac{\mathrm{d}r}{\mathrm{d}E}\cdot\frac{\mathrm{d}E}{\mathrm{d}e} = \frac{m\sin\gamma}{D}\cdot(E_f-E_0) \qquad (22)$$

$$\frac{\mathrm{d}^2 h}{\mathrm{d}e^2} = \sum_{i=3}^{n}(i-1)(i-2)a_i e^{i-3} = \frac{\mathrm{d}^2 r}{\mathrm{d}E^2}\cdot(E_f-E_0)^2 \qquad (23)$$

From Eq. (6), $\dfrac{\mathrm{d}^2 r}{\mathrm{d}E^2}$ can be calculated by:

$$\frac{\mathrm{d}^2 r}{\mathrm{d}E^2} = m\cdot\frac{\cos\gamma\cdot\frac{\mathrm{d}\gamma}{\mathrm{d}E}\cdot D - \frac{\mathrm{d}D}{\mathrm{d}E}\cdot\sin\gamma}{D^2} \qquad (24)$$

Besides, considering Eqs. (2), (3), (4) and (6), $\dfrac{\mathrm{d}D}{\mathrm{d}E}$ can be obtained by:

$$\frac{\mathrm{d}D}{\mathrm{d}E} = \frac{c_D S_r}{2}\cdot(\dot\rho_E V^2 + 2\rho V\cdot\dot V_E)$$

$$= \frac{c_D S_r}{2}\cdot(-\beta\rho\cdot\dot r_E\cdot V^2 + 2\rho V\cdot\dot V_E) \qquad (25)$$

$$= D\cdot(-\beta\cdot\frac{\mathrm{d}r}{\mathrm{d}E}+\frac{2\dot V_E}{V})$$

Combining Eqs. (24) and (25), $\dfrac{\mathrm{d}^2 r}{\mathrm{d}E^2}$ can be deduced as follows:

$$\frac{\mathrm{d}^2 r}{\mathrm{d}E^2} = m \cdot \frac{\cos\gamma \cdot \frac{\mathrm{d}\gamma}{\mathrm{d}E} \cdot D - \frac{\mathrm{d}D}{\mathrm{d}E} \cdot \sin\gamma}{D^2}$$

$$= m \cdot \frac{\cos\gamma \cdot \frac{\mathrm{d}\gamma}{\mathrm{d}E} \cdot D - D \cdot (-\beta \cdot \frac{\mathrm{d}r}{\mathrm{d}E} + \frac{2\dot{V}_E}{V}) \cdot \sin\gamma}{D^2} \quad (26)$$

$$= m \cdot \frac{\cos\gamma \cdot \frac{\mathrm{d}\gamma}{\mathrm{d}E} - (-\beta \cdot \frac{\mathrm{d}r}{\mathrm{d}E} + \frac{2\dot{V}_E}{V}) \cdot \sin\gamma}{D}$$

Then, from Eqs. (6) and (26), $\frac{\mathrm{d}\gamma}{\mathrm{d}E}$ can be calculated by:

$$\frac{\mathrm{d}\gamma}{\mathrm{d}E} = \left[\frac{PD}{m} + (\frac{2\dot{V}_E}{V} - \frac{\beta m \sin\gamma}{D})\sin\gamma \right] / \cos\gamma$$

$$= \frac{L\cos\sigma - (mg - \frac{mV^2}{r})\cos\gamma}{DV^2} \quad (27)$$

where $P = \frac{d^2 r}{dE^2}$, and the bank angle value can be calculated as follows:

$$|\sigma| = \left| \begin{array}{c} \arccos(\frac{PD^2 V^2}{mL\cos\gamma} - \frac{2(D + mg\sin\gamma) \cdot \sin\gamma}{L\cos\gamma} \\ -\frac{m\beta V^2 (\sin\gamma)^2}{L\cos\gamma} + \frac{mg\cos\gamma}{L} - \frac{mV^2 \cos\gamma}{Lr}) \end{array} \right| \quad (28)$$

When the current energy satisfies $E > E_s$, the objective function is used to predict the range-to-go error, and the bank angle value obtained by Eq. (28) is used as the initial value of the iteration link in the corrector process. The control instruction is iteratively obtained by the secant method, which is expressed as follows:

$$\sigma_c(k+1) = \sigma_c(k) - \frac{\sigma_c(k) - \sigma_c(k-1)}{s_p(k) - s_p(k-1)} \cdot [s_p(k) - s_c] \quad (29)$$

where σ_c is the bank angle value of the new guidance period; k represents the number of iterations; $s_p(k)$ is the predicted range-to-go kth iteration; s_c is the actual range-to-go at the current point in the predictor-corrector link.

Combining with Eq. (19), when the current energy satisfies $E > E_s$, the bank angle obtained by Eq. (28) is used as the initial value of the iteration in the predictor-corrector link, and the analytical calcula-

tion of the terminal range-to-go by Eq. (18) is selected as the objective function. At this time, the HGV is close to the target point, and the amount of calculation of the integral prediction method used to obtain the landing point has been greatly reduced. When $E \leq E_s$, the equidistant test method is used to calculate the bank angle. Different values of the bank angle with a certain interval distance around the bank angle obtained from Eq. (28) are selected to calculate the predicted landing point deviation, and then the bank angle with minimum deviation is taken as the output control command.

3.1.3 Adaptive guidance cycle

Unlike the common fixed guidance cycle in the traditional predictor-corrector method, our method adopts an adaptive guidance cycle strategy. The guidance cycle is calculated as follows:

$$\Delta T_{\mathrm{guide}} = \begin{cases} 200 - 20 * k_{\mathrm{guide}}, k_{\mathrm{guide}} < 10 \\ 10, k_{\mathrm{guide}} \geq 10 \end{cases} \quad (30)$$

where $\Delta T_{\mathrm{guide}}$ represents the actual guidance cycle and k_{guide} is the number of guidance cycles. The parameters in Eq. (30) are obtained from experience and can be adjusted according to actual reentry tasks.

3.2 Lateral guidance

Lateral guidance can use the heading angle deviation corridor to determine the sign of the inclination angle. The heading angle deviation corridor used in this study was as follows:

$$|\Delta\psi_{\mathrm{th}}| = \begin{cases} 10, & 6000 < V \leq V_0 \\ 15, & 3000 < V \leq 6000 \\ \frac{7}{1200}(V - 3000) + 15, 1800 < V \leq 3000 \\ 8, & V \leq V_f \end{cases} \quad (31)$$

where V_0 is the initial velocity of the reentry flight; V_f is the expected velocity at the terminal time; $|\Delta\psi_{\mathrm{th}}|$ represents the boundary value of the heading angle deviation. The heading angle deviation can obtained by $\Delta\psi = \psi - \psi_{\mathrm{los}}$, where ψ_{los} is the line of sight angle and can be calculated by:

$$\tan\psi_{\mathrm{los}} = \frac{\sin(\theta_f - \theta)}{\cos\phi\tan\phi_f - \sin\phi\cos(\theta_f - \theta)} \quad (32)$$

Then, the symbol of the bank angle can be ob-

tained by:

$$sgn(\sigma^i) = \begin{cases} -1, & \Delta\psi \geq |\Delta\psi_{th}(V)| \\ sign(\sigma^{i-1}), & \Delta\psi \in (-|\Delta\psi_{th}(V)|, |\Delta\psi_{th}(V)|) \\ 1, & \Delta\psi \leq -|\Delta\psi_{th}(V)| \end{cases} \tag{33}$$

Above all, the bank angle is given by:

$$\sigma = |\sigma_c| \cdot sgn(\sigma) \tag{34}$$

When $E < E_s$, the symbol and the magnitude of the bank angle are obtained by the equidistant test method. Therefore, there is no need to design an additional lateral guidance strategy.

3.3 Calculation of the altitude-energy profile

In section 3.1.2, a novel altitude-energy profile was proposed, which is used to calculate the bank angle, altitude, and velocity analytically. To obtain this profile, it is necessary to determine the value of $a_i, i = 1, 2, \cdots, n$, which requires n equations. Once the reentry mission is determined, the initial and terminal altitude, velocity and FPA are known, and from Eqs. (20) and (22), the following equations can be established:

$$h_0 = \sum_{i=1}^{n} a_i e_0^{i-1} \tag{35}$$

$$h_f = \sum_{i=1}^{n} a_i e_f^{i-1} \tag{36}$$

$$\frac{m\sin\gamma_0}{D_0}(E_f - E_0) = \sum_{i=2}^{n}(i-1)a_i e_0^{i-2} \tag{37}$$

$$\frac{m\sin\gamma_f}{D_f}(E_f - E_0) = \sum_{i=2}^{n}(i-1)a_i e_f^{i-2} \tag{38}$$

where h_0 and h_f are the initial and the terminal altitude, e_0 and e_f are the initial and the terminal non-dimensional energy, and $e_0 = 0, e_f = 1$, γ_0 and γ_f represent the initial and the terminal FPA, respectively. D_0 and D_f are the initial and the terminal drag, respectively.

With the aim of determining n parameters a, $n-4$ equations are still needed. $n-4$ points can be selected from $[e_0, e_f]$ and noted as $e_1, e_2, \cdots, e_{n-4}$, and the corresponding altitudes are $h_1, h_2, \cdots, h_{n-4}$, respectively. Then, the following equations can be obtained from Eq. (20):

$$h_j = \sum_{i=1}^{n} a_i e_j^{i-1}, j = 1, 2, \cdots, n-4 \tag{39}$$

where $e_j, j = 1, 2, \cdots, n-4$ are constants, and $h_j, j = 1, 2, \cdots, n-4$ are designed altitude parameters determined by an optimization algorithm.

Define $\boldsymbol{A} = [a_n, a_{n-1}, \cdots, a_2, a_1]^T$ and $\boldsymbol{H} = [h_0, h_1, h_2, \cdots, h_n, h_f, \frac{m\sin\gamma_0}{D_0}, \frac{m\sin\gamma_f}{D_f}]^T$. According to Eqs. (28)-(34), the n coefficients are calculated as follows:

$$\boldsymbol{A} = \boldsymbol{B}^{-1} \cdot \boldsymbol{H} \tag{40}$$

where

$$\boldsymbol{B} = \begin{bmatrix} e_0^{n-1} & \cdots & e_0^3 & e_0^2 & e_0 & 1 \\ e_1^{n-1} & \cdots & e_1^3 & e_1^2 & e_1 & 1 \\ e_2^{n-1} & \cdots & e_2^3 & e_2^2 & e_2 & 1 \\ & \cdots & & \cdots & & \\ e_{n-4}^{n-1} & \cdots & e_{n-4}^3 & e_{n-4}^2 & e_{n-4} & 1 \\ e_f^{n-1} & \cdots & e_f^3 & e_f^2 & e_f & 1 \\ (n-1)e_0^{n-2} & \cdots & 3e_0^2 & 2e_0 & 1 & 0 \\ (n-1)e_f^{n-2} & \cdots & 3e_f^3 & 2e_f & 1 & 0 \end{bmatrix}.$$

3.4 Algorithm framework

In this paper, the order of polynomial of Eq. (20) is set to five, which means $n = 6$. As a result, four parameters will be optimized:

$$\boldsymbol{X} = [V_1, V_2, h_1, h_2]^T \tag{41}$$

where two velocity parameters V_1, V_2 determine the AOA profile, and two height parameters h_1, h_2 determine the altitude-energy profile. The values of e_1 and e_2 corresponding to the h_1, h_2 can be selected randomly in $(0,1)$. To simplify the calculation, $e_1 = \frac{1}{3}, e_2 = \frac{2}{3}$ were set here. Combining with $e_0 = 0, e_f = 1$, Eq. (40) can be calculated easily with a light calculation burden.

In this method, an improved sparrow search algorithm (ISSA) is applied to optimize the four parameters. The SSA method is a novel and effective swarm intelligence optimization algorithm inspired by the foraging and anti-foraging behaviors of sparrows (Xue and Shen, 2020). In our previous study (Xu et al, 2021), ISSA showed better convergence

efficiency and global optimality than other PSO, WOA, and SSA. The sparrow swarm can be divided into discoverers and followers. The discoverers can find food areas and share the position with the other individual sparrows. The particle update strategy of ISSA is described in detail by Xu et al. (2021). Fig. 1 shows the framework of the segmented predictor-corrector guidance method.
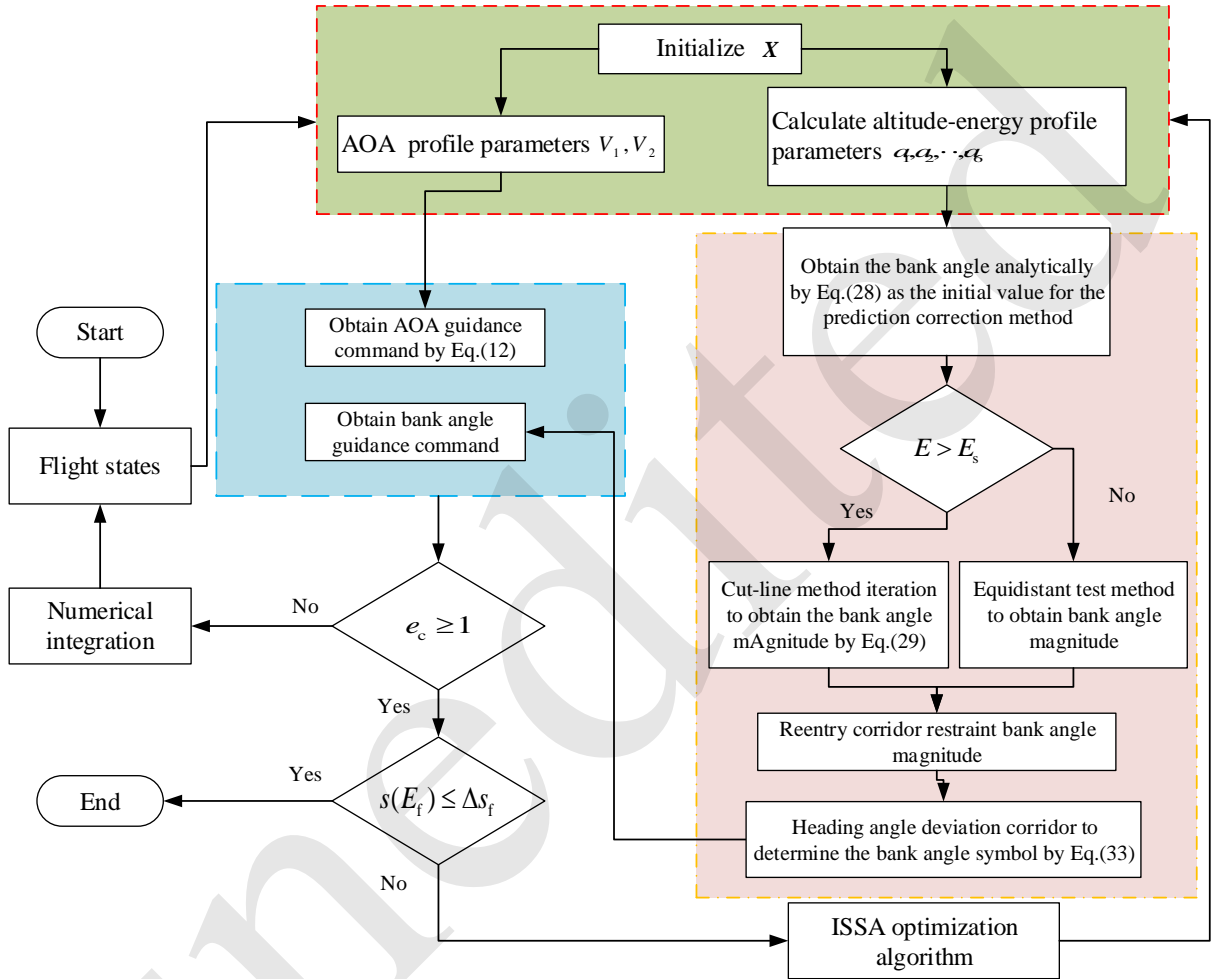

Fig. 1 Flowchart of the proposed novel guidance algorithm

When the flight process begins, the ISSA algorithm first provides an initial value for X, combines the current state of the aircraft, and uses Eq. (12) to calculate the AOA value. At the same time, based on the derivation in Section 3.3, Eq. (40) is used to obtain the parameters of the height energy profile. Then, Eq. (28) is used to obtain a good initial value for the prediction and correction iteration. It is judged whether the energy at the current moment is greater than the segmented energy threshold. If it is, the trapezoidal method is used to solve the amplitude of the roll angle. Otherwise, the equal distance test method is used to solve the amplitude of the roll angle guidance command. After that, the roll angle is used to re-enter the corridor, correcting the amplitude of the roll angle guidance command. The deviation corridor of the heading angle is used to determine the sign of the roll angle, obtaining a complete attack angle and roll angle guidance command. Furthermore, it is judged whether the current energy has reached the energy boundary of the mission. If it has not, integration needs to continue. If it has reached the energy boundary, it is judged whether the remaining flight distance error is within an allowable range.

If it is within range, simulation ends; if it is not, the remaining flight distance error is recorded, and ISSA is used to iteratively solve for the position of the next particle until an optimal height energy profile is obtained, while keeping the remaining flight distance error within an allowable range.

4 Simulation results and discussion

The CAV-H vehicle (Phillips, 2003) was used as the simulation object in this study to verify the effectiveness of the proposed method. The reference area of the HGV was about $0.484\,\text{m}^2$ and the mass about 907.2 kg. The constraints and some terminal conditions for all the reentry guidance simulations are listed in Table 1. All the path constraints and the control constraints should be satisfied strictly in the whole process.

Table 1 Parameter sets of the simulations

Constraints	Values	Terminal conditions	Values
n_{m}	$5g_0$	h_{f}	30km
q_{m}	400kPa	θ_{f}	$165°$
$\dot{Q}_{\text{m}}$	1200kW/m^2	ϕ_{f}	$55°$
α	$[10°, 25°]$	V_{f}	900m/s
σ	$[-80°, 80°]$	γ_{f}	$0°$

4.1 Testing of the proposed analytical segmented predictor-corrector reentry guidance method with adaptive guidance cycle

Six scenarios with different initial conditions were selected for investigation. The initial values set are listed in Table 2. The parameters of ISSA were set as follows: the population size $N = 30$; the maximum number of iterations $n_{\text{max}} = 20$; the discoverers and the warning sparrows each account for 20% of the population and $s_{\text{r}} = 0.8$.

Figs. 2-9 show the reentry guidance simulation results for the six scenarios. Because an analytical altitude-energy profile method was adopted, and the altitude profile could be obtained analytically, it can be seen from Figs. 2-3 that the terminal altitude and velocity constraints could be strictly satisfied for experiments with different initial altitudes and velocities. Fig. 4 shows the change in latitude and longitude. The proposed method could accurately guide the HGV to reach the target point exactly. From Table 3, the maximum landing error was 2.34 km and the minimum was 0.21 km. Fig. 5 shows that the reentry trajectory obtained by this algorithm can well meet the terminal FPA constraints. The AOA profile is designed as a linear piecewise function. Fig. 7 shows the bank angle profiles of the six simulation tasks obtained by the proposed algorithm. After entering the guidance stage, the adaptive guidance period was adopted, which affects the generation of the bank angle command. Fig. 8 shows the change of path constraints. The three path constraints of the trajectory obtained by the proposed algorithm were less than the maximum allowable value. The range-to-go changes are shown in Fig. 9. The range-to-go at the terminal moment was close to zero, meeting the allowable error range.
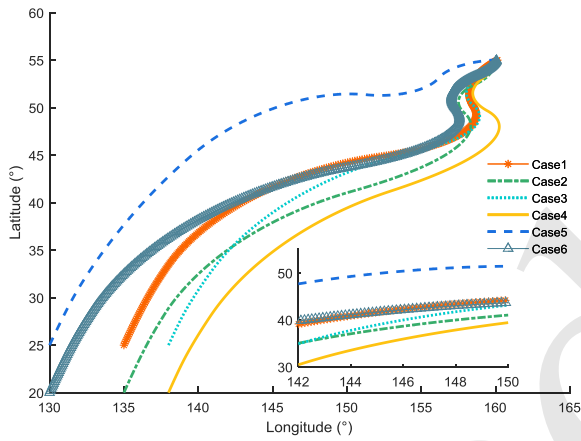
Table 2 Scenarios for simulations

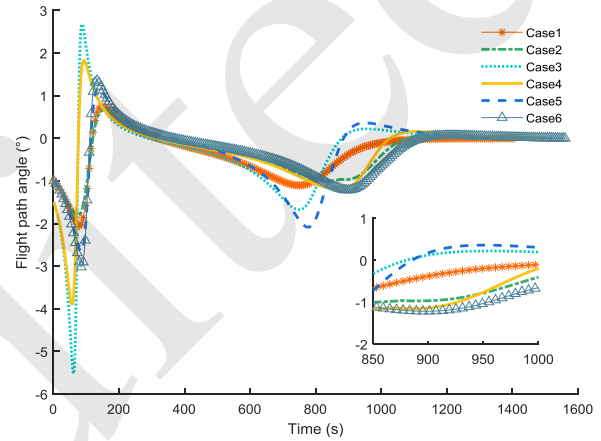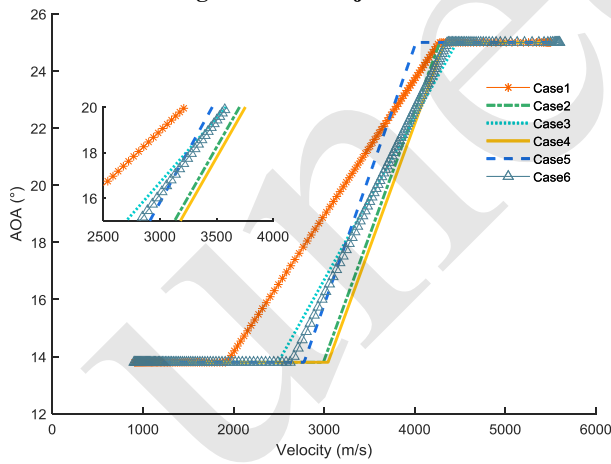| Initial	Altitude (km)	Longitude (/°)	Latitude (/°)	Velocity (m/s)	FPA (/°)
Case1	60	135	25	5500	-1
Case2	60	135	20	5400	-1
Case3	60	138	25	5400	-1.5
Case4	59	138	20	5500	-1.5
Case5	62	130	25	5500	-1
Case6	62	130	20	5600	-1
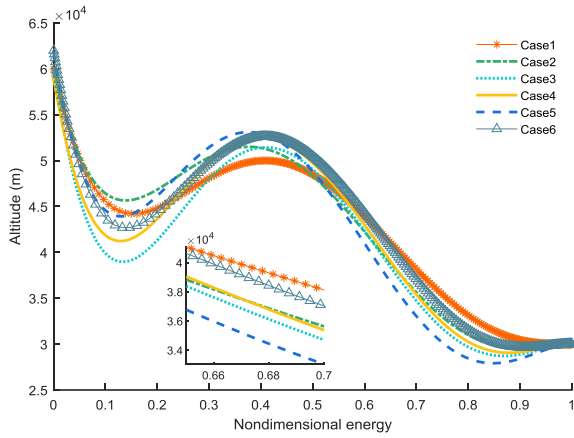
Fig. 2 Altitude-nondimensional energy profile
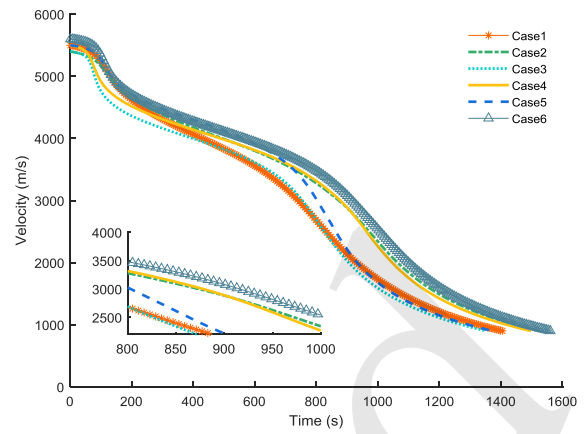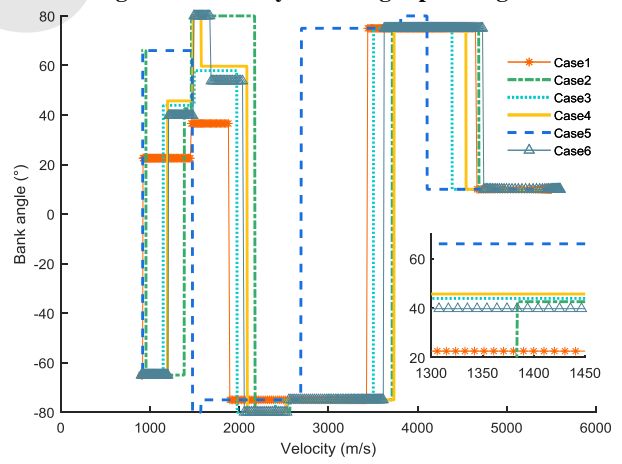

Fig. 3 Time history of the velocity

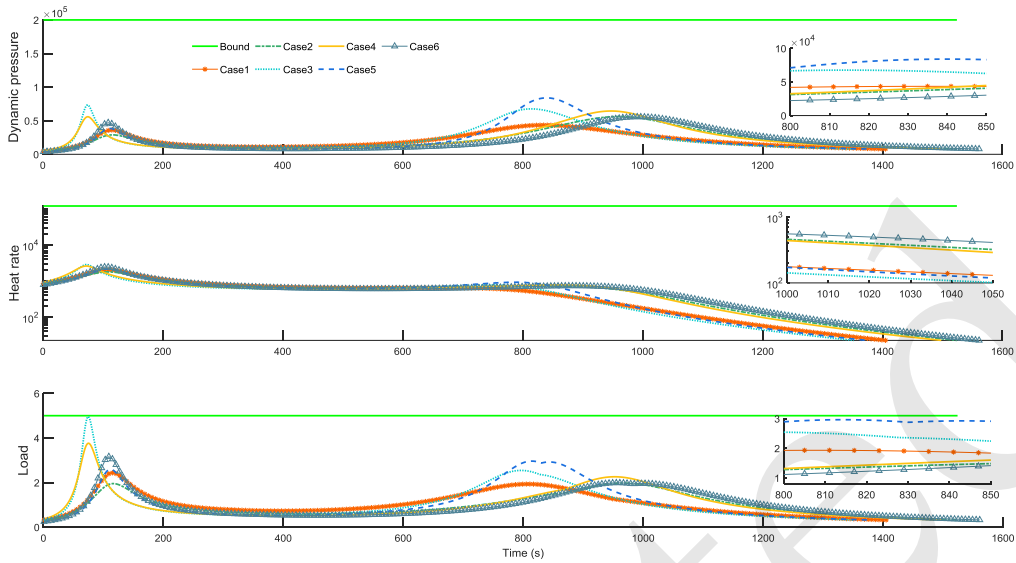**Fig. 4 Ground trajectories**

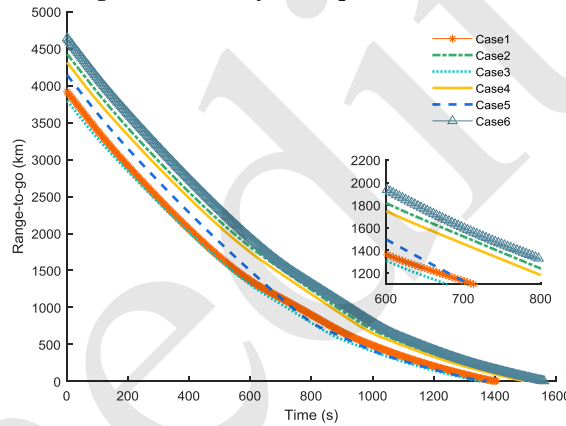**Fig. 5 Time history of the flight path angle**

Fig. 6 Time history of the AOA

Fig. 7 Time history of the bank angle

Fig. 8 Time history of the path constraints

Fig. 9 Time history of the range-to-go

Table 3 The results of simulations

Case	Terminal range errors (km)	Design parameters			
		V_1 (m/s)	V_2 (m/s)	h_1 (m)	h_2 (m)
1	1.73	4268.38	1923.57	49042.67	40084.94
2	2.89	4275.54	2991.13	51126.58	37727.16
3	3.73	4463.23	2491.83	49722.71	37114.04
4	5.79	4327.03	3042.62	51178.07	37778.65
5	4.56	4379.13	2260.11	52090.05	36031.29
6	5.24	4359.34	2635.96	51202.03	39404.40

Four optimized design parameters and terminal range-to-go values are listed in Table 3. The four parameter values are all in the constraint range, and the terminal range-to-go values of the six simulations were close to zero and within the allowable error range.

Above all, under the guidance of the control profile obtained by the proposed analytical segment-ed predictor-corrector guidance method, the HGV could be steered to the target point precisely with a safe trajectory.

4.2 Comparisons and discussion

To indicate the advantages of our proposed

method, three comparative experiments were performed. The proposed method is divided into three main strategies: analytical prediction of range-to-go, segmented prediction-correction guidance, and an adaptive guidance cycle. Therefore, three comparative experiments were set up as follows:

(1) Method 1 involved using the integral method to predict the landing point, segmented prediction-correction guidance, and adaptive guidance cycle.

(2) Method 2 was conducted using analytical prediction of the range-to-go, non-segmented prediction-correction guidance, and adaptive guidance cycle.

(3) Method 3 used analytical prediction of the range-to-go, segmented prediction-correction guidance, and a fixed guidance cycle.

The trajectories were calculated by the proposed method. The population of the ISSA was set as $N = 20$, the maximum iteration number was set as $n_{max} = 10$. Other parameters were the same as in case 1.

Figs. 10-17 show a comparison of results from the four methods. Figs. 10, 11, and 13 show that the terminal altitude, velocity, and FPA constraints were well satisfied. This is because the altitude-energy profile can naturally meet the terminal altitude and

velocity constraints. Fig. 14 shows the AOA profile met the designed linear piecewise function profile. Fig. 15 shows the bank angle profiles obtained by the four methods. Method 1 had a smaller range of bank angle changes. The change of range-to-go is shown in Fig. 16. Combined with Fig. 12, it can be seen that all four algorithms could accurately reach the target point to meet the allowable error of terminal range-to-go. The terminal range errors were 0.32 km for our proposed method, 1.54 km for Method 1, 1.66 km for Method 2, and 1.21 km for Method 3. The result shows the advantage of the high precision of the guidance method proposed in this study.

To compare the computational efficiency of the four algorithms, 20 experiments were carried out on the four methods, and the CPU time of each method was calculated. The results are shown in Fig. 18. Note that the population size in the Method 1 execution process was set to 10, $N = 10$, and the maximum number of iterations was set to 5, $n_{max} = 5$, due to the prolonged time taken by the analytical method to obtain the guidance trajectory. Table 4 shows the CPU time consumption of the four methods. The analytical segmented adaptive predictive correction guidance method proposed in this paper had a fast solving speed and potential suitability for online use.

Table 4 Statistical results and time cost

Time cost (s)	Best	Worst	Mean	Standard deviation
Proposed method	3.47	3.98	3.71	0.11
Method 1	6.25	45.29	14.64	11.04
Method 2	3.28	4.07	3.69	0.19
Method 3	3.48	3.93	3.70	0.14
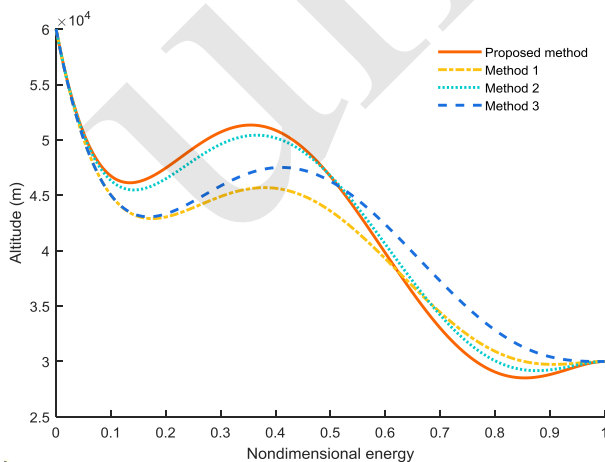
Fig. 10 Altitude-nondimensional energy profile
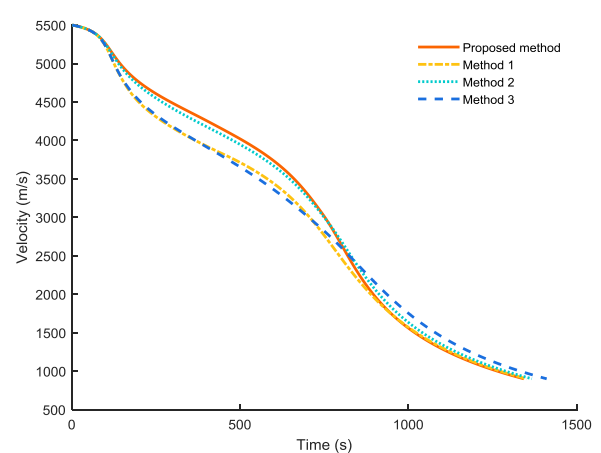
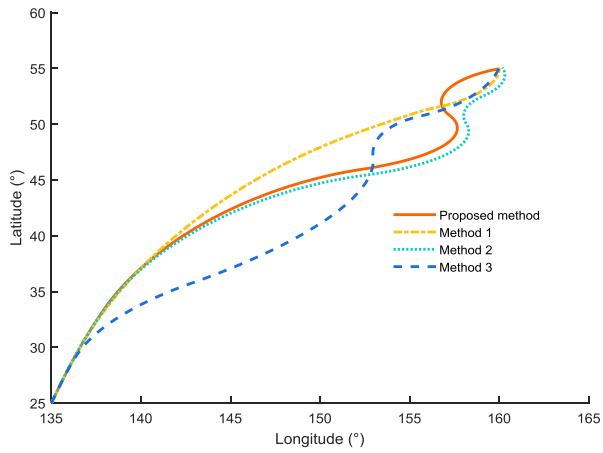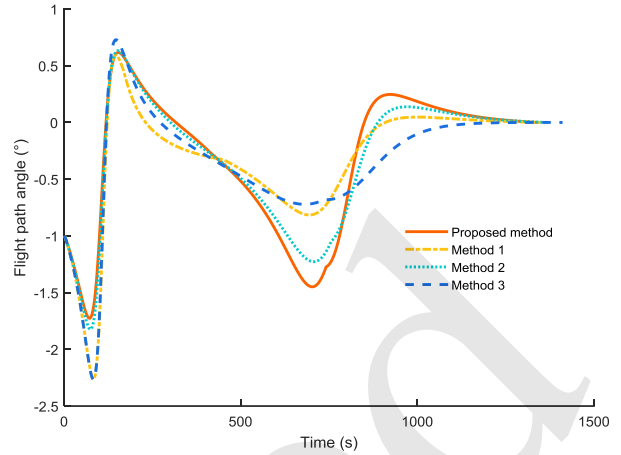**Fig. 11 Time history of the velocity**

Fig. 12 Ground trajectories

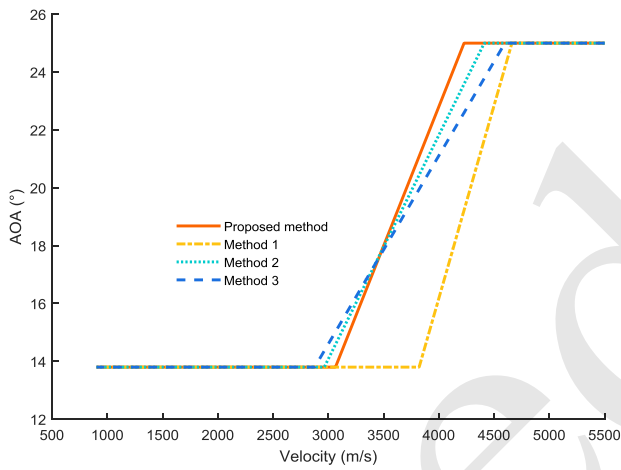**Fig. 13 Time history of the flight path angle**

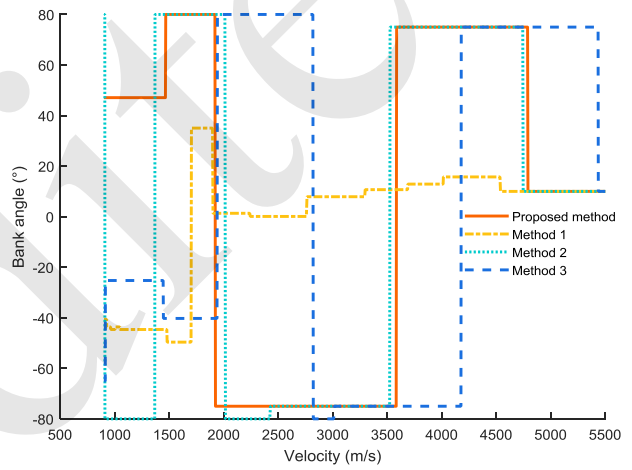**Fig. 14 Time history of the AOA**

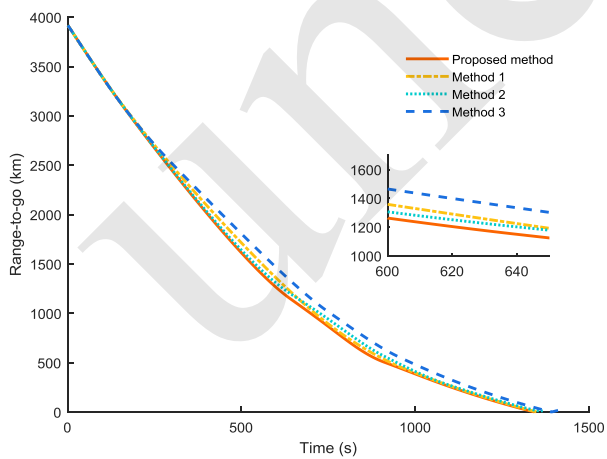**Fig. 15 Time history of the bank angle**

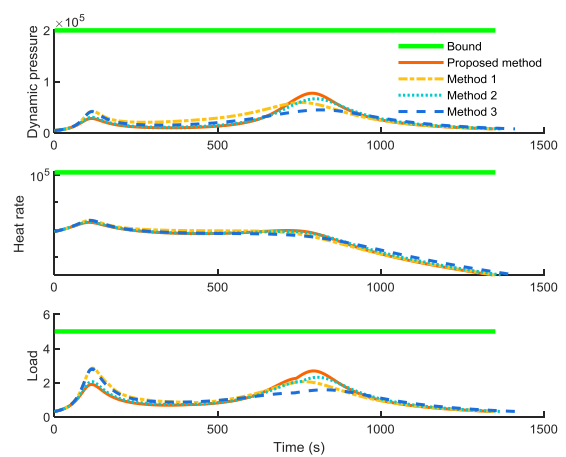**Fig. 16 Time history of the range-to-go**
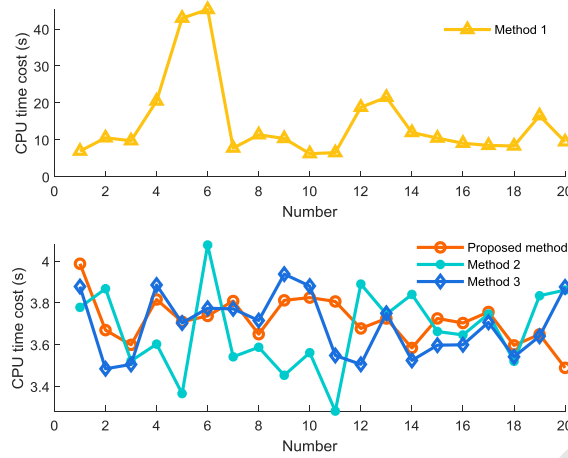

Fig. 17 Time history of the path constraints

Fig. 18 CPU time cost

4.3 Monte-Carlo simulations

To demonstrate the robustness of the guidance method proposed in this paper, 200 independent cases of Monte-Carlo simulations based on case 1 were conducted. The disturbances obeyed a Gaussian distribution with the values of 3σ listed in Table 5. A tolerance value of terminal range error was set as $\Delta s_f = 15$km in these simulations.

Table 5 3σ value of the Gaussian distribution

Initial disturbances	3σ value
Altitude (/m)	1000
Longitude (/°)	1
Latitude (/°)	1
Velocity (m/s)	200
Flight path angle (/°)	0.5

Figs. 19-24 illustrate the results of the simulations. Figs. 19-21 show the terminal altitude, velocity, and ground track, respectively. 200 independent experiments verified that our proposed guidance method could meet terminal constraints and reach the target accurately. Fig. 22 shows the distribution of landing points. Combined with Fig. 23, it shows that the landing points could meet the allowable deviation of 15 km, and most of the landing points were concentrated within 10 km. Fig. 24 shows the CPU time distribution for 200 experiments. The statistical results of the terminal range errors and time cost are listed in Table 6.

From the Monte-Carlo simulations results, it is obvious that the proposed guidance solution has strong robustness and stability under the set disturbances.

Table 6 Statistical results of terminal range errors and time cost

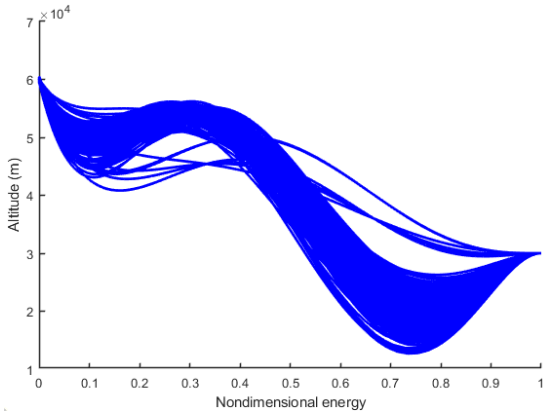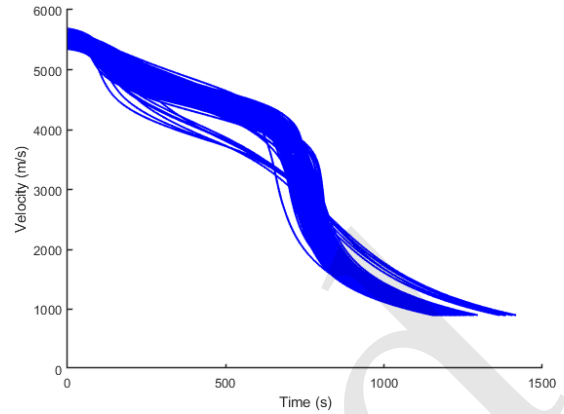| Values	Best	Worst	Mean	Standard deviation
Terminal range errors (km)	1.48	14.89	7.74	5.38
Time cost (s)	2.82	3.52	3.06	0.11

Fig. 19 Time history of the altitude

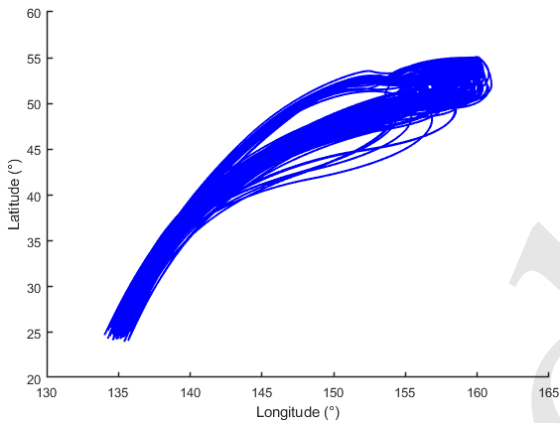**Fig. 20 Time history of the velocity**

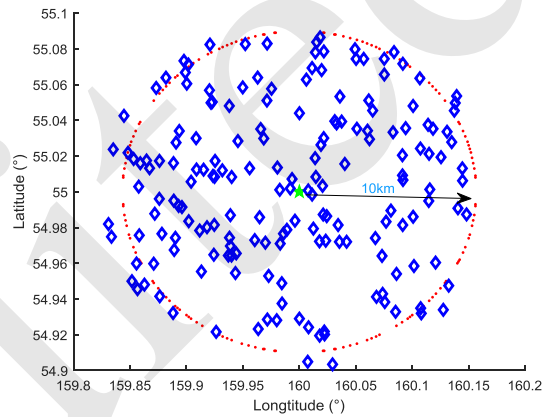**Fig. 21 Ground track**
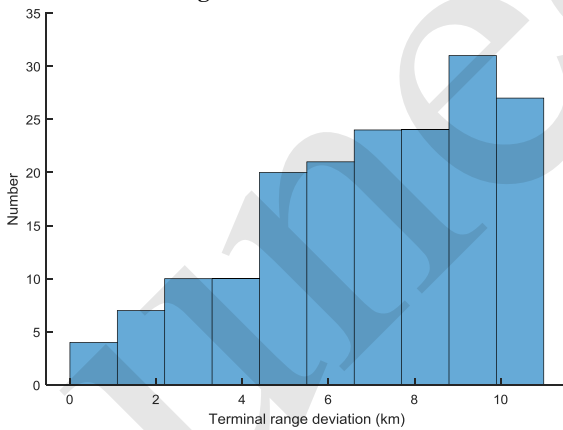

Fig. 22 Terminal location distribution

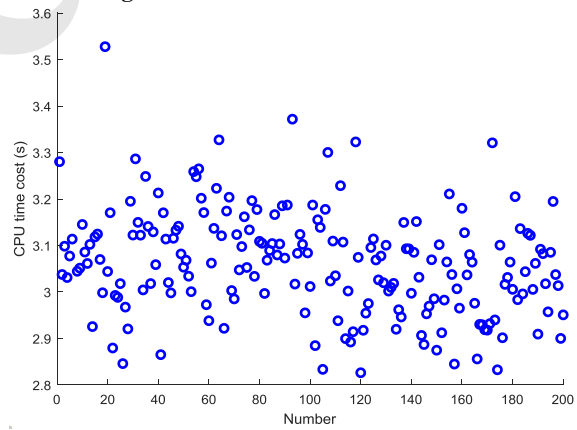**Fig. 23 Histogram of the terminal range deviation**

Fig. 24 CPU time cost

5. Conclusions

The novel analytical segmented guidance method for HGV proposed in this paper has distinct computational efficiency advantages.

1. Based on the altitude-energy profile defined in the paper, the bank angle can be roughly obtained with an analytical form. This can be used as the initial value of the bank angle in the predictor-corrector link.

2. An analytical segmented prediction method of range-to-go is proposed. This method greatly improves the efficiency of range-to-go prediction, reducing the calculation time from 14.64s to 3.71s compared to the integral method for predicting range-to-go. Additionally, the strategy of the adaptive guidance cycle further optimizes the calculation of guidance commands.

3. Simulation results from various scenes, comparative experiments of four methods, and Monte-

Carlo simulation show that our proposed method has good accuracy, fast calculation speed, and robustness, indicating good potential for online application.

In our future work, the algorithm will be applied to online trajectory reconstruction and reentry tasks involving target points.

Acknowledgments

Author contributions

Hui XU designed the research and wrote the first draft of the manuscript. Guangbin CAI and Chaoxu MU provided the corresponding guidance. Xin LI helped organize the manuscript. Hao WEI revised and edited the final version.

Conflict of interest

Hui XU, Guangbin CAI, Chaoxu MU, Xin LI and Hao WEI declare that they have no conflict of interest.

References

An K, Guo ZY, Huang W, et al., 2022. Leap trajectory tracking control based on sliding mode theory for hypersonic gliding vehicle. *Journal of Zhejiang University-SCIENCE A (Applied Physics & Engineering)*, 23(3):188-207. https://doi.org/10.1631/jzus.A2100362.

Chen K, Liang WC, Liu MX, et al., 2020. Comparison of geomagnetic aided navigation algorithms for hypersonic vehicles. *Journal of Zhejiang University-SCIENCE A (Applied Physics & Engineering)*, 21(8):673-683.
https://doi.org/10.1631/jzus.A1900648.

Gao Y, Cai GB, Zhang SX, et al., 2019. Reentry maneuver guidance for hypersonic glide vehicles under multiple no-fly zones. *Journal of Ordnance Equipment Engineering*, 40(8):32-39.
https://doi.org/10.11809/bqzbgcxb2019.08.0 (in Chinese).

Gao Y, Cai GB, Xu H, et al., 2020. Reentry maneuver guidance of hypersonic glide vehicle under virtual multi-tentacle detection, *Acta Aeronautica et Astronautica Sinica*, 41(11): 623703.
https://doi.org/10.7527/S10006893.2019.23703 (in Chinese).

Gao Y, Cai GB, Yang XG, et al., 2019. Improved tentacle-based guidance for reentry gliding hypersonic vehicle with no-fly zone constraint. IEEE Access, 7:119246-58. https://doi.org/10.1109/ACCESS.2019.2936974.

Joshi A, Sivan K, Amma S, 2007. Predictor-corrector reentry guidance algorithm with path constraints for atmospheric entry vehicles, *Journal of Guidance Control and Dynamics*, 30(5):1307-1318. https://doi.org/10.2514/1.26306.

Lu P, 2008. Predictor-corrector entry guidance for low lifting vehicles, *Journal of Guidance Control and Dynamics*, 31 (4): 1067-1075. https://doi.org/10.2514/1.320.

Lu P, 2014. Entry guidance: a unified method, *Journal of Guidance Control and Dynamics*, 37(3): 713-728. https://doi.org/10.2514/1.626.

Li MM, Hu J, 2018. An approach and landing guidance design for reusable launch vehicle based on adaptive predictor-corrector technique, *Aerospace Science and Technology*, 75: 13-23.
https://doi.org/10.1016/j.ast.2017.12.037.

Liang ZX, Li QD, Ren Z, 2017. Virtual terminal-based adaptive predictor-corrector entry guidance. *Journal of Aerospace Engineering*, 30(4): 04017013-04017022. https://doi.org/10.1061/(ASCE)AS.1943-5525.0000716.

Liang ZX, Zhu SY, 2021. Constrained predictor-corrector guidance via bank saturation avoidance for low L/D entry vehicles. *Aerospace Science and Technology*, 109:106448-106457.
https://doi.org/10.1016/j.ast.2020.106448.

Pan L, Peng S, Xie Y, et al., 2019. 3D guidance for hypersonic reentry gliders based on analytical prediction, *Acta Astronautics*, 42: 164-175.
https://doi.org/10.1016/j.actaastro.2019.07.039.

Phillips TH, A common aero vehicle (CAV) model, Description and Employment guide, Schafer corporation for AFRL and AFSPC, 27 January 2003.

Shen ZL, Lu P, 2003. Onboard generation of three-dimensional constrained entry trajectories, *Journal of Guidance Control and Dynamics*, 26(1):111-121. https://doi.org/10.2514/2.5021.

Tauqeer ul Islam RIZVI S, He LS, Xu DJ, 2015. Optimal trajectory and heat load analysis of different shape lifting reentry vehicles for medium range application. *Defence Technology*, (11): 350-361.
http://doi.org/10.1016/j.dt.2015.06.003.

Wang T, Zhang H, Tang G, 2017. Predictor-corrector entry guidance with waypoint and no-fly zone constraints, *Acta Astronautics*, 138:10-18. http://doi.org/10.1016/j.actaastro.2017.05.009.

Wang T, Zhang H, Zeng L, et al., 2017. A robust predictor-corrector entry guidance, *Aerospace Science and Technology*, 66: 103-111.
http://doi.org/10.1016/j.ast.2017.03.010.

Wang X, Guo J, Tang SJ, et al., 2019. Time-cooperative entry guidance based on analytical profile. *Acta Aeronautica et Astronautica Sinica*, 40(3): 322565-322576. http://doi.org/10.7527/S10006893.2018.22565 (in Chinese).

Xue S, Lu P, 2010. Constrained predictor-corrector entry guidance. *Journal of Guidance Control and Dynamics*, 33(4): 1273-1281. http://doi.org/10.2514/6.2009-5767.

Xia Y, Shen G , Zhou L, et al., 2015. Mars entry guidance based on segmented guidance predictor-corrector algorithm. *Control Engineering Practice*, 45:79-85. http://doi.org/10.1016/j.conengprac.2015.08.006.

Xu H, Cai GB, Zhang SX, 2021. Modified aerodynamic coefficient fitting models of hypersonic gliding vehicle in reentry phase. *Journal of Astronautics*, 42(9): 1139-1149.

http://doi.org/10.3873/j.issn.1000-1328.2021.09.009.

Xu H, Cai GB, Zhang SX, et al., 2022. Hypersonic reentry optimization by using improved sparrow search algorithm and control parametrization method. *Advance in Space Research*, 69(6):2512-2524

http://doi.org/10.1016/j.asr.2021.12.030.

Xue J, Shen B, 2020. A novel swarm intelligence optimization approach: sparrow search algorithm, *Systems Science & Control Engineering*, 8(1): 22-34. https://doi.org/10.1080/21642583.2019.1708830.

Yong E, Qian W, He K, 2014. An adaptive predictor-corrector reentry guidance based on self-definition way-points. *Aerospace Science and Technology*, 39: 211-221. http://dx.doi.org/10.1016/j.ast.2014.08.004.

Yu WB, Chen WC, Jiang Z, et al., 2018. Analytical entry guidance for No-fly zone avoidance. *Aerospace Science and Technology*, 72:426-42. http://dx.doi.org/10.1016/j.ast.2017.11.029.

Zhang XY, Wang GH, Song ZY, et al., 2015. Hypersonic sliding target tracking in near space. *Defence Technology*, (11): 370-381. http://dx.doi.org/10.1016/j.dt.2015.05.004.

Zhang HX, Gong ZF, Cai GB, et al., 2019. Reentry tracking control of hypersonic vehicle with complicated constraints, *Journal of Ordnance Equipment Engineering*, 40(1):7-12. https://doi.org/10.11809 / bqzbgcxb2019.01.001.

Zhang JL, Liu K, Fan YZ, et al., 2021. A piecewise predictor-corrector reentry guidance algorithm with No-fly zone avoidance. *Journal of Astronautics*, 42(01):122-131. https://doi.org/10.3873/j.issn.1000-1328.2021.01.01.

Zeng L, Zhang H, Zheng L, 2018. A three-dimensional predictor-corrector entry guidance based on reduced-order motion equations, *Aerospace Science and Technology*, 73: 223-231. https://doi.org/10.1016/j.ast.2017.12.009.

Zeng XF, Wang JY, Wang XH, 2013. Gliding guidance based on energy and analytical predictor-corrector. *Systems Engineering and Electronics*, 35(12): 2582-2589. https://doi.org/10.3969/j.issn.1001-506X.2013.12.23.

Zhou HY, Wang XG, Cui NG, 2020. Glide guidance for reusable launch vehicles using analytical dynamics, Aerospace Science and Technology, 98:105678-96.https://doi.org/10.1016/j.ast.2019.105678.